Biased Quasiballistic Spin Torque Magnetization Reversal

S. Serrano-Guisan,[1,*] K. Rott,[2] G. Reiss,[2] J. Langer,[3] B. Ocker,[3] and H. W. Schumacher[1,†]

[1]*Physikalisch-Technische Bundesanstalt, Bundesallee 100, D-38116 Braunschweig, Germany*

[2]*Department of Physics, University of Bielefeld, Universitätsstrasse 25, 33615 Bielefeld, Germany*

[3]*Singulus Nano Deposition Technologies GmbH, Hanauer Landstrasse 103, D-63796 Kahl am Main, Germany*

(Received 15 May 2008; published 19 August 2008)

We explore the ultrafast limit of spin torque magnetization reversal time. Spin torque precession during a spin torque current pulse and free magnetization ringing after the pulse is detected by time-resolved magnetotransport. Adapting the duration of the pulse to the precession period allows coherent control of the final orientation of the magnetization. In the presence of a hard axis bias field, we find optimum quasiballistic spin torque magnetization reversal by a single precessional turn directly from the initial to the reversed equilibrium state.

DOI: 10.1103/PhysRevLett.101.087201 PACS numbers: 85.75.Dd, 72.25.−b, 75.60.Jk

A spin-polarized current transfers spin angular momentum to the magnetization M of a ferromagnet and thereby exerts a so-called spin torque (ST) on M [1]. ST can, e.g., excite spin waves [2] and can lead to current-induced magnetization reversal [3]. Promising applications are ST oscillators and magnetic random access memories (MRAM) [4]. ST precession has been intensively studied in the frequency domain [5]. Time domain measurements have underlined the importance of ST precession for ST reversal and showed that M generally undergoes multiple precessional turns during reversal [6]. In contrast, ultrafast field-induced magnetization reversal can occur by a half precessional turn only [7]. During this so-called ballistic magnetization reversal, the duration of a transverse field pulse matches one-half of the precession period leading to an optimized reversal directly from the initial to the reversed equilibrium during the pulse. A corresponding ballistic ST reversal could allow ultrafast and yet efficient future ST devices. Here we explore the ultrafast limit of ST-induced magnetization reversal. We detect ST precession and ST-induced free precession by time-resolved magnetoresistance measurements. Adapting the duration of the current pulse to the ST precession period allows coherent control of the ringing and thus of the final orientation of M. In the presence of a hard axis bias field, ultrafast quasiballistic ST reversal directly from the initial to the final equilibrium orientation by a single precessional turn is observed.

Experiments are performed on nanopillars of MgO magnetic tunneling junctions (MTJs) with a resistance area product of $\sim 6.5\ \Omega\ \mu m^2$. MTJs are sputter deposited in a Singulus NDT Timaris cluster tool. The deposition sequence is 3 nm Ta/90 nm CuN/5 nm Ta/20 nm PtMn/2 nm $Co_{60}Fe_{20}B_{20}$/0.75 nm Ru/2 nm $Co_{60}Fe_{20}B_{20}$/1.3 nm MgO/3 nm $Co_{60}Fe_{20}B_{20}$/10 nm Ta/30 nm Cu/8 nm Ru. The MgO barrier is formed in three steps. First, 0.9 nm of metallic Mg is deposited and oxidized in 0.01 Torr oxygen for 300 s. Then 0.4 nm of metallic Mg is deposited on top. The completed stack is annealed for 90 minutes at 360 °C in a 1 T field and lithographically patterned into 140 nm × 285 nm wide elliptic nanopillars.

Figure 1(a) shows a room temperature tunneling magnetoresistance (TMR) loop with the field swept along the easy (long) axis of the ellipsoid (x axis). The magnetization M of the upper CoFeB free layer reverses, while the magnetization M_P of the lower pinned layer remains along the negative x orientation. The loop shows well-defined reversal from the parallel low resistance to the antiparallel high resistance state with a TMR of 140%. Figure 1(b) shows a switching asteroid compiled from x axis hysteresis loops taken at various y axis fields. The sample shows quasisingle domain reversal with a uniaxial anisotropy field of $\mu_0 H_K \approx 15$ mT. In static measurements, such

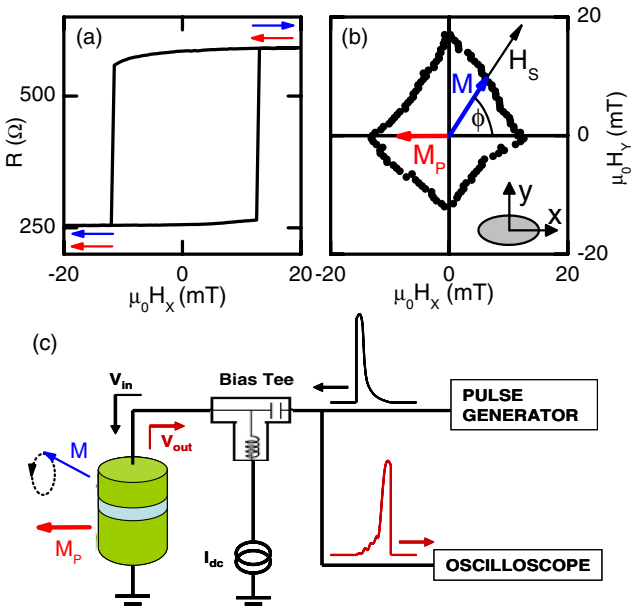

FIG. 1 (color online). (a) Free layer easy axis TMR hysteresis loop and (b) switching asteroid. Configuration of H_S, M, and M_P is sketched. (c) Experimental setup for electrical detection of ST precession.

devices show a critical current density for ST magnetization reversal of about $j_C = 7\text{–}9 \times 10^6$ A/cm^2.

The dynamics of the M are detected at room temperature by time-resolved magnetoresistance measurements in reflection as shown in Fig. 1(c). The MTJ nanopillars terminate a 50 Ω coaxial line. A current pulse from a pulse generator is split by a power splitter, and one-half of the pulse is injected into the MTJ, while the other half is terminated by a 18 GHz sampling oscilloscope. Because of impedance mismatch, the current pulse is partially reflected by the MTJ. The reflected pulse is again split by the power splitter, and half of the reflected signal is recorded by the sampling oscilloscope, while the other half is terminated in the pulse generator. ST excitation of M by the current pulse leads to an angular excursion of M and thus a change of the TMR that can be detected in the reflected signal. To separate the TMR change from the background of the reflected pulse, a weak dc detection current ($I_{dc} = 200\ \mu$A) is applied to the MTJ through a bias tee [8]. Subtraction of two oscilloscope traces measured at $\pm I_{dc}$ yields the TMR signal change without the background of the reflected pulse. The dc detection current allows the measurement of ST precession during the ST current pulse and of free precession (ringing) after the pulse. Therefore, in contrast to earlier studies [6], also nonequilibrium orientations of M after pulse decay can be evidenced and investigated. The oscilloscope traces are taken at a 100 kHz pulse repetition rate and averaged over up to 2000 traces to reduce noise. Additionally, static fields up to $\mu_0 H_S = 30$ mT in arbitrary in-plane angles ϕ are applied as sketched in Fig. 1(b). Current pulses with 160 ps–5 ns duration with effective current densities up to $j = 9 \times 10^6$ A/cm^2 are applied.

Figure 2 shows typical measurements of time-resolved ST precession during the pulse (a) and free precession of M after the pulse (b) of the device in Fig. 1. The TMR voltage change is plotted vs time. Figure 2(a) shows the voltage change during the rise of a 5 ns pulse of $j = 3.2 \times 10^6$ A/cm^2. For the positive j, spin-polarized electrons flow from the pinned to the free layer favoring the low resistance (parallel) state. M is on the low resistance side of the asteroid with the easy axis component m_X parallel to M_P as $\mu_0 H_S = 22.8$ mT $> \mu_0 H_K$ is applied along $\phi = -114°$ (inset sketch). The data show a damped voltage oscillation on top of a rising background. The oscillation is due to ST precession of M, while the background mainly results from an effective tilt $\Delta\phi$ of M towards M_P due to ST. Figure 2(c) shows the TMR voltage change during and after ST excitation by a 180 ps pulse of $j = 9 \times 10^6$ A/cm^2 with $\mu_0 H_S = 22.8$ mT and $\phi = 84°$ (inset sketch). Here a voltage oscillation after the decay of the pulse is observed. Now M relaxes by free precession (ringing) towards its equilibrium orientation along H_S.

From the data in Figs. 2(a) and 2(c), an exponential background (gray line) is subtracted yielding the precession data on the right in Figs. 2(b) and 2(d). Fitting the precession data by an exponentially damped sinusoid (gray line) yields the precession frequency f and the effective damping α_{eff} [9]. The frequencies of free and ST precession are $f_{\text{free}} = 4.05$ GHz and $f_{\text{ST}} = 5.25$ GHz, respectively. This difference is mainly due to the different orientations ϕ of H_S and M in the two cases. For low applied fields ($H_S \approx H_K$), the anisotropy gives rise to an angular dependence of f with a minimum at $\pm 90°$ leading to a lower frequency for the ringing at 84°. α_{eff} is calculated taking into account the saturation magnetization $\mu_0 M_S = 1.6$ T yielding $\alpha_{\text{eff}}^{\text{ST}} = 0.0136 \pm 0.001$ and $\alpha_{\text{eff}}^{\text{free}} = 0.011 \pm 0.002$. For free precession $\alpha_{\text{eff}}^{\text{free}}$ equals the Gilbert damping α [10]. $\alpha_{\text{eff}}^{\text{ST}}$ results from competition of Gilbert damping and ST. Here an increased effective damping ($\alpha_{\text{eff}}^{\text{ST}} > \alpha$) is found as expected for the low resistance configuration with j favoring the low resistance state [11].

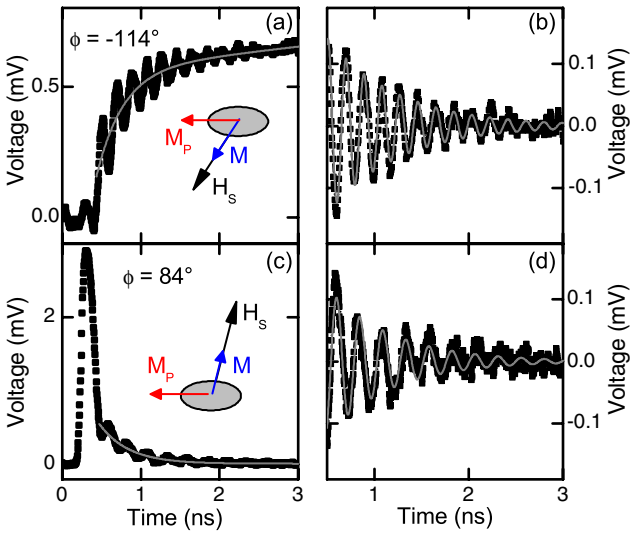

FIG. 2 (color online). Time-resolved TMR signal of ST and free precession. $\mu_0 H_S = 22.8$ mT. (a) ST precession during the rise of a 5 ns pulse of $j = 3.2 \times 10^6$ A/cm^2 at $\phi = -114°$. (c) Free precession after excitation by a 180 ps pulse of $j = 9 \times 10^6$ A/cm^2 at $\phi = 84°$. (b),(d) Precession data after background subtraction [gray line in (a),(c)]. Parameters are derived from fitting a damped sinusoid (gray line).

As mentioned above, the ringing results from nonequilibrium orientation of M upon pulse decay. For ultrafast ST-MRAM, such excitation must be avoided. As relaxation to equilibrium can take several nanoseconds, the effective reversal time including ringing is considerably longer than the write pulse thereby limiting write performance. Furthermore, excitation of M can evoke uncontrolled thermally activated back switching to the initial state thus reducing switching reliability.

Figure 3(a) shows suppression of the ringing after a ST pulse by proper selection of the pulse parameters. The TMR signal is plotted for six different pulse durations $T_{\text{Pulse}} = 450\text{–}1250$ ps. The data are taken in the low resistance state ($\mu_0 H_S = 24$ mT, $\phi = -104°$) with $j = -7.8 \times 10^6$ A/cm^2 favoring the high resistance (antipar-

allel) state. The curves are offset for clarity. The dotted gray lines mark the onset and the decay of the excitation pulse. During pulse application, a strong ST precession of $f_{ST} = 3.3$ GHz is observed. Note that now $\alpha_{\text{eff}}^{\text{ST}} = 0.0098 \pm 0.001 < \alpha$ for the inverted current polarity favoring the high resistance state [1,11]. Ringing is observed for $T_{\text{Pulse}} = 450$, 770, and 1100 ps (gray curves), whereas for $T_{\text{Pulse}} = 600$, 930, and 1250 ps (black curves) practically no ringing is present. For the latter, the ringing and thus the final orientation of M upon pulse decay are coherently controlled. Here T_{Pulse} approximately equals an integer multiple of the ST precession period $T_{\text{Pulse}} \approx \text{nT}_{\text{Prec}}$. During the pulse, M undergoes $n = 2, 3, 4$ precessional turns starting from H_S and is again aligned along H_S upon pulse decay [lower sketch in Fig. 3(b)], and the ringing is suppressed. For the gray curves, the ST pulse terminates after approximately n-1/2 precessional turns. At this point of the trajectory, M has the maximum tilt off equilibrium as shown in the upper sketch in Fig. 3(b). M thus relaxes towards H_S after the pulse by free precessional ringing.

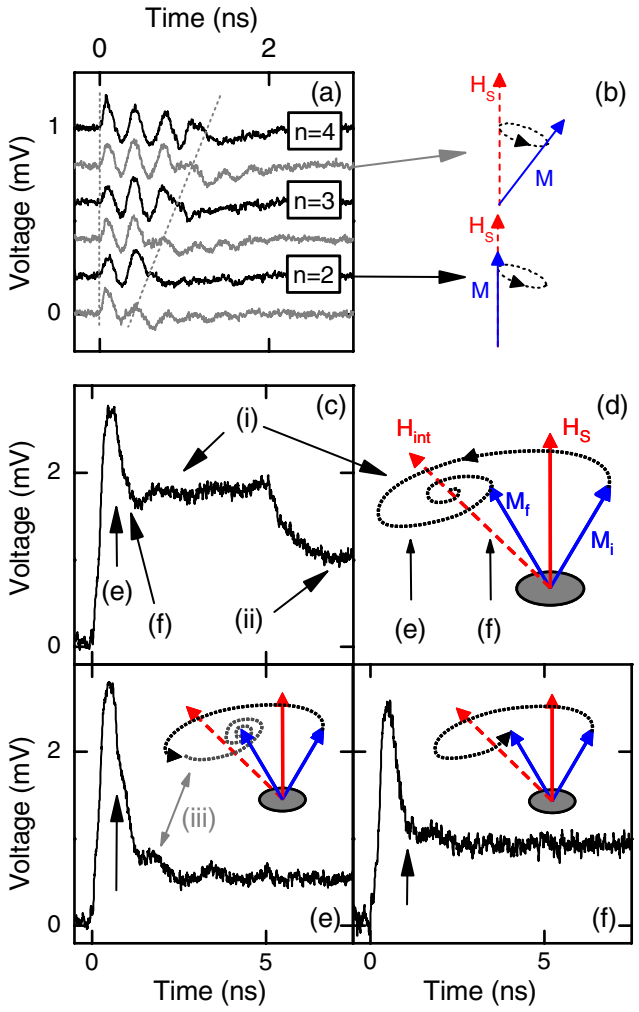

FIG. 3 (color online). (a),(b) Suppressed ringing of M by variation of ST pulse duration. $\phi = -104°$, $\mu_0 H_S = 24$ mT, $j = -7.8 \times 10^6$ A/cm^2. $T_{\text{Pulse}} = 450$, 600, 770, 930, 1100, and 1250 ps. Graphs are offset for clarity. For the black curves, ringing is coherently controlled after $n = 2, 3, 4$ full precessional turns as sketched in (b). (c)–(f) Biased precessional ST reversal by $j = 2.5 \times 10^6$ A/cm^2 with $\mu_0 H_S = 10$ mT along the in-plane hard axis (y axis). (c) ST reversal by 5 ns pulse. ST precession (i) and relaxation to reversed state (ii) after the pulse is observed. (d) Sketch of magnetic configurations and reversal trajectory. (e) ST reversal by 730 ps with strong ringing (iii) and low switching reliability. (f) Quasiballistic ST reversal by 1.1 ns pulse. The pulse terminates in the precession minimum of (c). Optimized reversal occurs by one full precessional turn.

Such coherent control of M can also be used to realize ultrafast ST magnetization reversal. In the following, we present measurements of ST reversal in an in-plane transverse (y axis) bias field $\mu_0 H_S = 10$ mT. Such biased ST switching has been proposed to improve the switching reliability for subnanosecond ST reversal [12]. The magnetic configurations are sketched in Fig. 3(d). The experiments are carried out on a similar device having a higher uniaxial anisotropy of $\mu_0 H_K = 21.5$ mT. Reversal from antiparallel (high resistance) to parallel (low resistance) by ST pulses of $j = 2.5 \times 10^6$ A/cm^2 is studied. The initial state M_i has a positive easy axis component ($m_X > 0$), and H_S tilts M to approximately $\phi = 60°$. The final state M_f is symmetric to the hard axis. For the sampling measurements, M is reset into the initial state by a 10 μs ST reset pulse of $j \approx -7 \times 10^6$ A/cm^2 prior to the ST measurement pulse. Figure 3(c) shows biased ST switching by a 5 ns pulse. The measured TMR voltage change can be explained the sketched trajectory in Fig. 3(d). At the pulse inset, a precessional overshoot is observed followed by a damped precession of M [arrow (i)]. Here M overcomes the hard axis and precesses about the intermediate effective field H_{int} resulting from competition of H_S, H_K, and ST. As ST favors the parallel state, this intermediate orientation is stronger tilted towards M_P than the final reversed orientation M_f. After decay of the ST pulse, M relaxes from H_{int} to M_f (ii) by free precession. Note that precessional oscillations are not resolved but appear as an exponential decay to the final voltage. Here the precession is dephased due to thermal activation of M after the 5 ns high current density pulse, and the oscillations are smeared out in the sampling measurements. Note that the bias and the strong initial precession already allow efficient ST reversal by j being about 3 times smaller than j_C derived from static experiments.

Figures 3(e) and 3(f) show reversal by shorter pulses of the same j. The pulses decay to zero after 730 ps and 1.1 ns, respectively. For the 730 ps pulse (e), the ST precession ends during the initial precessional overshoot marked by the arrow (e) in Figs. 3(c) and 3(d). In the data, the pulse decay is observed as a kink in the decay of the overshoot (black arrow). At this moment, M has reversed and is oriented between H_{int} and M_f. After the pulse, ringing is found (iii) as M relaxes to M_f by free precession [inset in Fig. 3(e)]. Therefore, despite the subnanosecond

switching pulse, the effective magnetization reversal time from the initial to the final equilibrium takes several nanoseconds. In addition, the final voltage of the reversed state is almost a factor of 2 lower than in Fig. 3(c). Here the reversal probability is reduced to about 50%. After the pulse, M is strongly excited and can stochastically switch back to M_i involving thermal activation. The sampling measurements average over successful and unsuccessful switching and the final voltage is reduced. Note that the ringing (iii) could, in principle, also be due to relaxation towards M_i after the unsuccessful switching. For unsuccessful switching, M stochastically overcomes the hard axis involving thermal activation. Such thermal activation, however, evokes a considerable dephasing of the precession which should smear out the oscillations in the sampling measurements.

Figure 3(f) shows magnetization reversal by a 1.1 ns ST pulse. Now the ST pulse terminates in the voltage minimum after the overshoot [see arrow (f) in Figs. 3(c) and 3(d)]. The pulse decays at the same time as the overshoot (arrow), and the TMR voltage immediately equals the final value of the reversed state in Fig. 3(c) evidencing highly reliable reversal. No significant ringing of M after the overshoot is found, and no exponential decay speaking for a dephased precession is present. Here M reverses directly from M_i to M_f on an optimum ultrafast quasiballistic trajectory. During ST pulse application, M undergoes only a single precessional turn about H_{int}. At the moment of pulse decay, M is oriented near M_f and thus near the reversed equilibrium as sketched in the inset. This biased quasiballistic ST reversal represents the fundamental ultrafast limit of the magnetization reversal time for the given field and current configuration.

Note that, in contrast to field-induced quasiballistic reversal [7], no ST reversal by a half precessional turn has been found. During the initial overshoot, M already passes near M_f after a half precessional turn, but no reliable reversal has been found for the corresponding pulse duration. Here M most probably has a significant out-of-plane component and is thus highly excited inhibiting ballistic ST reversal by a half precessional turn.

In conclusion, we have demonstrated biased quasiballistic ST magnetization reversal in MTJ nanopillars as used in present ST-MRAM prototypes. Such ballistic reversal could allow for low current, ultrafast, and highly reliable future ST devices.

We acknowledge funding by DFG within Priority Program "Ultrafast Magnetization Processes."

*santiago.serrano-guisan@ptb.de
†hans.w.schumacher@ptb.de

[1] J. C. Slonczewski, J. Magn. Magn. Mater. **159**, L1 (1996); L. Berger, Phys. Rev. B **54**, 9353 (1996).
[2] M. Tsoi *et al.*, Phys. Rev. Lett. **80**, 4281 (1998); M. Tsoi *et al.*, Nature (London) **406**, 46 (2000).
[3] E. B. Myers *et al.*, Science **285**, 867 (1999); J. A. Katine *et al.*, Phys. Rev. Lett. **84**, 3149 (2000); J. Grollier *et al.*, Appl. Phys. Lett. **78**, 3663 (2001).
[4] Y. Huai *et al.*, Appl. Phys. Lett. **84**, 3118 (2004).
[5] S. I. Kisilev *et al.*, Nature (London) **425**, 380 (2003); W. H. Rippard *et al.*, Phys. Rev. Lett. **92**, 027201 (2004); S. Kaka *et al.*, Nature (London) **437**, 389 (2005); J. Grollier, V. Cros, and A. Fert, Phys. Rev. B **73**, 060409(R) (2006); A. A. Talapurkar *et al.*, Nature (London) **438**, 339 (2005); J. C. Sankey *et al.*, Nature Phys. **4**, 67 (2008); H. Kubota *et al.*, *ibid.* **4**, 37 (2008).
[6] R. H. Koch, J. A. Katine, and J. Z. Sun, Phys. Rev. Lett. **92**, 088302 (2004); N. C. Emley *et al.*, *ibid.* **96**, 247204 (2006); I. N. Krivorotov *et al.*, Science **307**, 228 (2005); Y. Acremann *et al.*, Phys. Rev. Lett. **96**, 217202 (2006); G. D. Fuchs *et al.*, *ibid.* **96**, 186603 (2006); T. Devolder *et al.*, *ibid.* **100**, 057206 (2008); I. N. Krivorotov *et al.*, Phys. Rev. B **77**, 054440 (2008).
[7] S. Kaka and S. E. Russek, Appl. Phys. Lett. **80**, 2958 (2002); Th. Gerrits *et al.*, Nature (London) **418**, 509 (2002); H. W. Schumacher *et al.*, Phys. Rev. Lett. **90**, 017201 (2003); **90**, 017204 (2003).
[8] Variation of $I_{\mathrm{dc}} = 50$–$300\ \mu$A does not significantly change the detected precession speaking for a noninvasive measurement.
[9] J. Miltat, G. Albuquerque, and A. Thiaville, Top. Appl. Phys. **83**, 1 (2002).
[10] L. Landau and E. Lifshitz, Phys. Z. Sowjetunion **8**, 153 (1935); T. L. Gilbert, Phys. Rev. **100**, 1243 (1955).
[11] M. D. Stiles and J. Miltat, Top. Appl. Phys. **101**, 225 (2006); J. Z. Sun, Phys. Rev. B **62**, 570 (2000).
[12] T. Devolder *et al.*, Phys. Rev. B **75**, 064402 (2007).